STRÄTLINGITE AND CALCIUM HEMICARBOALUMINATE HYDRATE IN BELITE-CALCIUM SULPHOALUMINATE CEMENT

FEI SONG, ZHENGLEI YU, FENGLING YANG, #YUNFEI LIU, ##YINONG LU

State Key Laboratory of Materials-Oriented Chemical Engineering, College of Materials Science and Engineering, Nanjing Tech University, Nanjing 210009, China

#E-mail: yfliu@njtech.edu.cn
##E-mail: yinonglu@njtech.edu.cn

Submitted July 8, 2014; accepted December 7, 2014

Keywords: Belite-calcium sulphoaluminate, Hydration, Strätlingite, Calcium hemicarboaluminate hydrate

Belite-calcium sulphoaluminate (BCSA) cement is a promising low-CO_2 alternative to ordinary Portland cement. With high water cement ratio, phase compositions of the BCSA pastes at different curing ages were investigated via X-ray diffraction (XRD) and differential scanning calorimetry (DSC). Large amounts of water accelerated the hydration reaction significantly and substantial ettringite ($C_6A\check{S}_3{\cdot}H_{32}$, AFt) was generated in the early stages. With the carbonation of AFt in the later stages, lots of strätlingite (C_2ASH_8) and calcium hemicarboaluminate hydrate ($C_4A\check{C}_{0.5}H_{12}$, H_c) formed after curing age of 28 days. The microstructure of C_2ASH_8 and H_c in the BCSA pastes were observed and confirmed via a scanning electron microscope (SEM) and an energy dispersive X-ray spectrometer (EDS). The results indicated that C_2ASH_8 was thick hexagonal plate product and H_c was thin sheet-like product. C_2ASH_8 and H_c would stack together respectively in the later stages of hydration. In addition, spherical aluminum hydroxide (AH_3) and rod-like AFt were also observed.

INTRODUCTION

Calcium sulphoaluminate (CSA) cement is manufactured by sintering mixtures of limestone, bauxite and gypsum (C$\check{S}$·2H) at a temperature of about 1250°C [1, 2]. It has good performance of rapid hardening, high strength, low alkali and so on [3, 4]. However, the compression strength of CSA cement decreases in the later age [5]. Bauxite as one of the main raw materials is too expensive. Therefore, high-performance belite-calcium sulphoaluminate (BCSA) cement is developed. The long-term strength and durability of concrete made from BCSA cement can potentially exceed those of other cements [6, 7]. Manufacturing BCSA cement produces less CO_2 than ordinary Portland cement and fully utilizes industrial by-products, such as fly sah, steelmaking slags, scrubber sludge and so on [8-12].

The main minerals in the BCSA cement are belite (C_2S) and yeelimite ($C_4A_3\check{S}$). It may also contain other minor phases such as ferrite, maynite and excess anhydrite (C$\check{S}$) [13]. The main hydration products of BCSA cement are similar to that of the CSA cement. The hydrates are ettringite ($C_6A\check{S}_3{\cdot}H_{32}$, AFt), monosulfate ($C_4A\check{S}{\cdot}H_{12}$, AFm), hydrated calcium silicate (C–S–H), amorphous aluminum hydroxide (AH_3) and so forth [5, 14, 15].

Strätlingite (C_2ASH_8) is an important hydration product of cement in the later stages [16, 17]. C_2ASH_8 is also known as "hydrated gehlenite" [18]. C_2ASH_8 might be responsible for the strength recovery in high-alumina cement (HAC) [19, 20]. To promote C_2ASH_8 formation, zeolites or silica fume was added to HAC cement and plate-like C_2ASH_8 was observed in HAC pastes [20, 21].

Calcium hemicarboaluminate hydrate ($C_4A\check{C}_{0.5}H_{12}$, H_c) can form when the calcite (C$\check{C}$) is low or absent in cement pastes but the H_c microstruture has not been reported [16, 22]. In fact, H_c belongs to AFm systems whose anion can be replaced by hydroxy, sulfate, carbonate and so on [23]. Especially, C_2ASH_8 is also a variant of AFm systems [24].

C_2ASH_8 and H_c have been also detected by many researchers in BCSA pastes but the microstructure has not been examined in detail. In this paper, to accelerate the hydration reaction, massive water was added to BCSA cement. C_2ASH_8 and H_c microstructure were examined. Such research data are necessary to understand C_2ASH_8 and H_c.

Cement nomenclature will be used, i.e.; C = CaO, S = SiO_2, $\check{S}$ = SO_3, A = Al_2O_3, $\check{C}$ = CO_2, H = H_2O

EXPERIMENTAL

Materials and methods

BCSA cement prepared as an industrial trial but not commercially available was studied. The chemical compositions of the BCSA cement were obtained by X-ray fluorescence spectrometry as shown in Table1.

Table 1. Chemical compositions of the BCSA cement (wt. %).

CaO	Al_2O_3	SO_3	SiO_2	MgO	TiO_2	Fe_2O_3	Others
48.24	24.56	6.98	16.43	0.56	0.60	2.22	0.41

The BCSA cement was milled to a Blaine fineness between 400 and 500 m^2/kg. The BCSA pastes were prepared using a water/cement ratio of 2.0. The BCSA cement blended with proper water was cast into a beaker and stored in a curing chamber at a temperature of 20°C ± 1°C and relative humidity was 95 % ± 5 %. After curing for 1, 3, 7 and 28 days, the BCSA pastes which had been filtered were respectively stopped by soaking in an excess of ethanol for 24 h and dried in a vacuum dessicator. Finally, part of the samples was ground for various tests.

Characterization

The X-ray diffraction patterns for the BCSA cement and pastes were obtained using an X-ray diffractometer (XRD, Smartlab-3kw, Rigaku Ltd, Japan) using Cu Ka radiation (λ = 0.15405 nm) running in a reflection geometry (θ/θ) at room temperature. A scanning speed of 5° min^{-1} with a step size of 0.02° was used to examine the samples. The acquisition range was from 5° to 45° 2θ. The X-ray tube was operated at 40 kV and 30 mA.

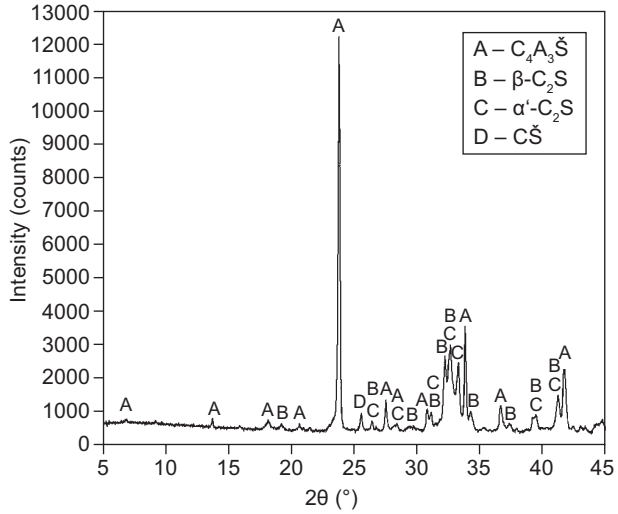

Figure 1. XRD pattern for the BCSA cement.

A thermal analysis was performed via differential scanning calorimetry (DSC, DSC 204, NETZSCH Co., Germany). The temperature was varied under N_2 atmosphere from 50°C to 300°C at a heating rate of 10° min^{-1}.

A scanning electron microscope (SEM, JSM-6510, JEOL Ltd, Japan) equipped with a W-filament and operated under an accelerating voltage of 15 kV was used to observe the samples microstructure. The samples were coated with a very thin layer of gold to increase their electrical conductivity.

The elemental compositions of hydration products with the characteristic morphologies were acquired using an energy dispersive X-ray spectrometer (EDS, NS7, Thermo Fisher Scientific Co., America).

RESULTS AND DISCUSSION

Phase compositions and microstructure of the BCSA cement

The XRD pattern for the BCSA cement is shown in Figure 1. The main phases of the BCSA cement are $C_4A_3Š$ and C_2S. $C_4A_3Š$ has an orthorhombic structure. The crystal structures for C_2S are in the β and α′ forms. Both $C_4A_3Š$ and C_2S possess good crystallinity. Moreover, the BCSA cement also contains small amounts of CŠ.

Figure 2 shows the SEM images and EDS patterns of the BCSA cement. There are many polygonal particles with a diameter around 2 μm as shown in Figure 2a. The EDS pattern (Figure 2b) indicated that the elemental compositions of polygonal particle (P 1) were Al, O, S and Ca. The Au signal arose from the sample surface coating used to elevate the electrical conductivity. Therefore, the polygonal particle was $C_4A_3Š$. From Figure 2c, spherical substance with a diameter of 1 ~6 μm was detected. The EDS pattern (Figure 2d) indicated that the elemental compositions of the spherical substance (P 2) were significant Si, O, Ca and a little Al. Therefore, the spherical substance was C_2S and it was doped with a little Al_2O_3. The grain size of main phases in BCSA cement was small.

Phase compositions of the BCSA pastes

The XRD patterns for the BCSA pastes with water/cement ratio of 2.0 at different curing ages are given in Figure 3. After curing age of 1 day, CŠ was completely dissolved and small amounts of unreacted CŠ·2H which was the hydration product of CŠ was found in the BCSA pastes. AFt formed in large scale according to Equation 1 but there was still small amounts of unreacted $C_4A_3Š$ in the pastes [16]. Massive water significantly accelerated the hydration reaction. Furthermore, AFm and AH_3 was also present according to Equation 2 [25, 26].

$$C_4A_3Š + 2CŠ + 38H \rightarrow AFt + 2AH_3 \quad (1)$$

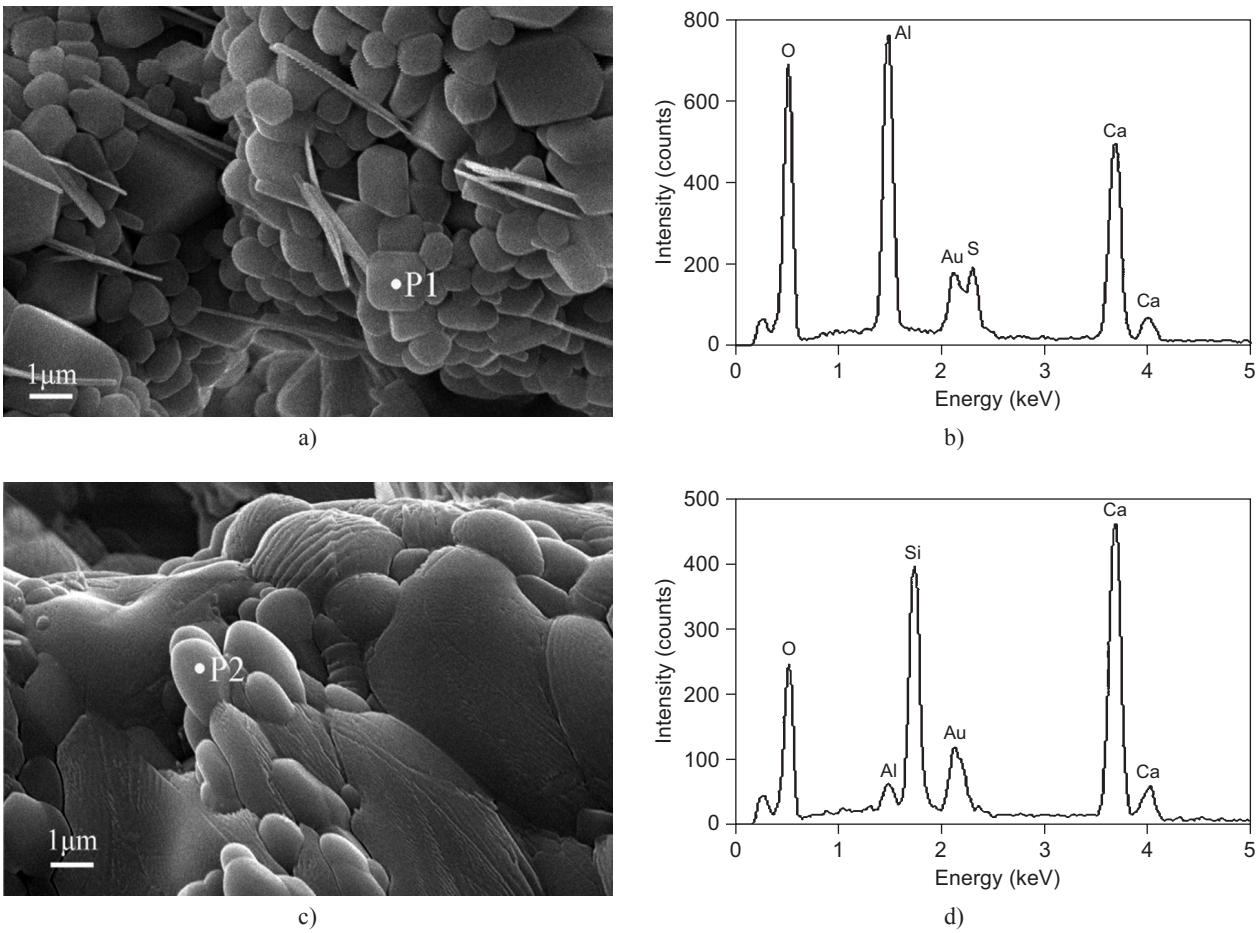

Figure 2. SEM images and EDS patterns of the BCSA cement: a), c) SEM images of the BCSA cement, b), d) EDS patterns for P 1 and P 2 respectively.

$$C_4A_3\check{S} + 18H \rightarrow AFm + 2AH_3 \quad (2)$$

Small amount of hydrated calcium aluminate (CAH_{10}) was present in the BCSA pastes after curing age of 3 days and it was the hydration product of calcium aluminate (CA). Crystallinity of a little CA may be poor so it can not be detected by XRD. Both $C_4A_3\check{S}$ and $C\check{S}\cdot 2H$ were fully reacted after curing age of 3 days. Especially, due to the existence of carbon dioxide in the air and water, small amounts of H_c was found in the BCSA paste after curing age of 3 days.

After curing age of 7 days, small amounts of C_2ASH_8 formed according to Equation 3 [22]. Quantity of AFm and H_c increased slightly. Small amounts of $C\check{S}\cdot 2H$ was found again because the AFt carbonation reaction started as shown in Equation 4 [14, 27].

$$C_2S + AH_3 + 5H \rightarrow C_2ASH_8 \quad (3)$$

$$AFt + 3\check{C} \rightarrow 3C\check{C} + 3C\check{S}\cdot 2H + AH_3 + 23H \quad (4)$$

Due to the continuous decomposition of AFt, a significant reduction of AFt was found after cuing age of 28 days. It revealed that massive water significantly

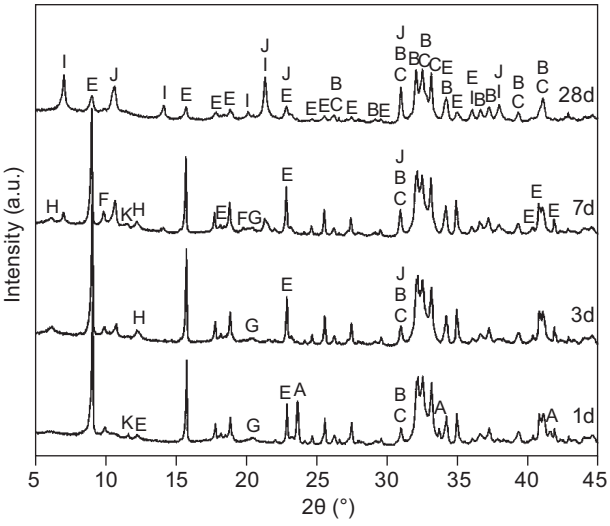

Figure 3. XRD patterns for the BCSA pastes with water cement ratio of 2.0 at different curing ages. (A – $C_4A_3\check{S}$; B – β-C_2S; C – α'-C_2S; E – AFt; F – AFm; G – AH_3; H – CAH_{10}; I – C_2ASH_8; J – H_c; K – $C\check{S}\cdot 2H$).

accelerated the AFt carbonation reaction. The main carbonation product of AFt, CČ was not detected by XRD but lots of H_c was generated. This can be explained by the fact that CČ benefits the formation of H_c [16]. With the existence of CŠ·2H, AH_3 reacted with calcium hydroxide (CH) which was the hydration products of C_2S illustrated in Equation 5 [16]. Therefore, small amounts of CŠ·2H disappeared again after curing age of 28 days. C_2S reacted further with AH_3 according to Equation 3 so the intensity of the main peaks of C_2S decreased apparently and great deal of C_2ASH_8 formed after curing age of 28 days.

$$AH_3 + 3CH + 3C\check{S}\cdot 2H + 20H \rightarrow AFt \quad (5)$$

A broad band between 20° and 21° indicative of AH_3 revealed that AH_3 was amorphous or micro-crystalline after curing age of 1, 3 and 7 days. For curing 28 days, AH_3 band overlapped with the C_2ASH_8 band. In this case, the presence of AH_3 in the BCSA pastes could not be determined requiring further testing via thermal analysis.

Thermal analysis of the BCSA pastes

The XRD results are also verified by the DSC data (Figure 4). The endothermic peak near 100°C belongs to dehydration of AFt and CAH_{10} [28]. From the XRD analysis, the CAH_{10} content was relatively small. Therefore, absorbing heat which increased and then decreased at the temperature around 100°C was mainly caused by the dehydration of AFt. It revealed that the amount of AFt increased in the first 3 days but from the seventh day to the twenty eighth day, the amount decreased because of the carbonation reaction.

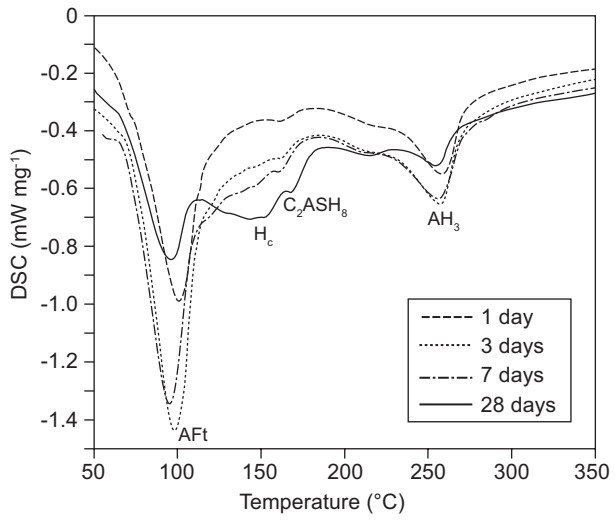

Figure 4. DSC curves for the BCSA pastes with water cement ratio of 2.0 at different curing ages.

Meanwhile, AH_3 (about 260°C) followed the same rule. AH_3 was generated after curing age of 1 day and it achieved significant growth after curing age of 3 days according to Equation 1, 2. After curing age of 7 days, the amount of AH_3 decreased slightly. After curing age of 28 days, the amount of AH_3 decreased significantly according to Equation 3 but AH_3 did not vanish in the BCSA pastes.

Absorbing heat quantity increased with ongoing hydration at 150 - 200°C because various hydration products were generated, for example AFm, H_c and C_2ASH_8 [17, 22, 29]. Especially, after curing age of 28 days, lots of Hc (about 150°C) and C_2ASH_8 (about 170°C) were produced [18, 22].

Microstructure of C_2ASH_8 and H_c in the BCSA pastes

From XRD results, after curing age of 7 and 28 days, C_2ASH_8 and H_c formed intensively so the microstructure of these curing age pastes were examined via SEM and EDS. Several typical morphologies of C_2ASH_8 and H_c were observed and confirmed as shown in Figure 5.

Figure 5a shows thick hexagonal plate-like substance precipitates together with rod-like AFt and villous spherical AH_3 (confirmed by EDS) after curing age of 7 days. Figure 5b indicated that the elemental compositions of plate-like substance (P 3) were Al, Si, O and Ca, so the plate-like substance was C_2ASH_8. The result is similar to that of F. Puertas [30].

From Figure 5c, thin sheet-like product surrounded by rod-like AFt and gel was observed after curing age of 7 days. The elemental compositions of the thin sheet-like product (P 4) were C, Al, O and Ca (Figure 5d), so the thin sheet-like product was H_c.

After curing age of 28 days, accumulated thick plate-like product covered by gel is detected as shown in Figure 5e. EDS pattern (Figure 5f) indicated that the elemental compositions of P 5 were Al, Si, O and Ca, so accumulated plate-like product was C_2ASH_8. It revealed that C_2ASH_8 would stack together in the later stages.

After curing age of 28d, lamellar structure substance covered by gel which is a mixture of C-S-H and AH_3 (confirmed by EDS) is observed (Figure 5g). Figure 5h indicated that the elemental compositions of P 6 were C, Al, O and Ca. The lamellar structure substance was H_c. It is speculated that the thin sheet-like H_c stacks together with each other forming the lamellar structure in the early stages and the lamellar H_c will also gather together in the later stages.

Although C_2ASH_8 and H_c belong to AFm systems or a variant of AFm systems, they have different morphologies. C_2ASH_8 and H_c gather together in the later stages of hydration and they are always surrounded by various hydrates.

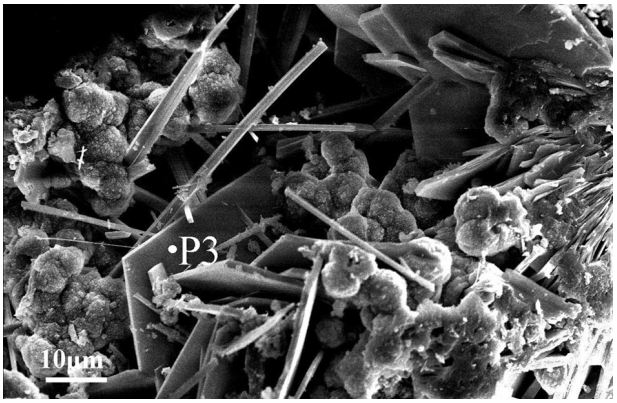

a)

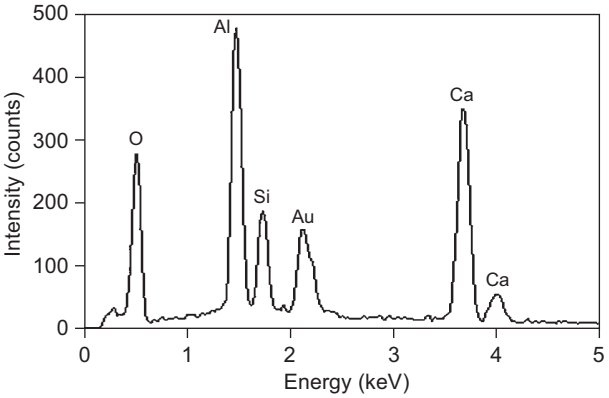

b)

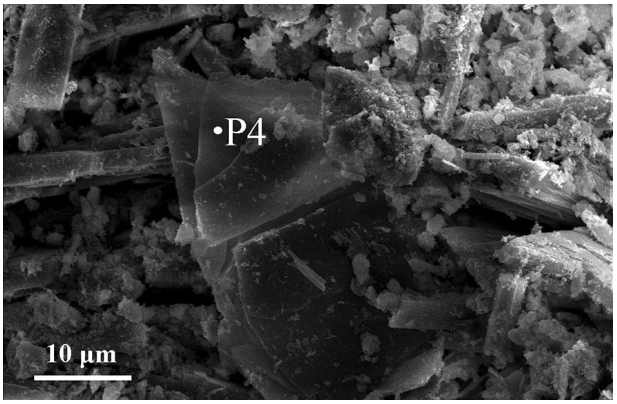

c)

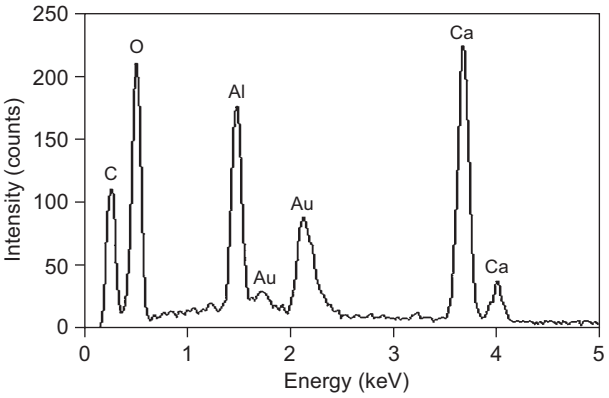

d)

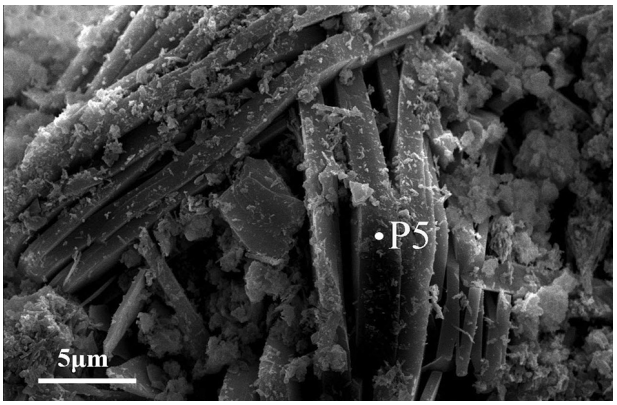

e)

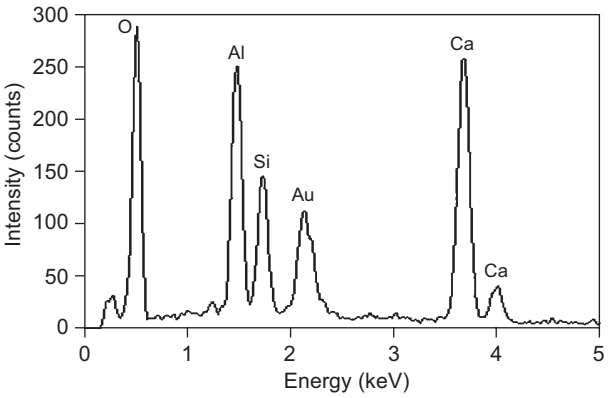

f)

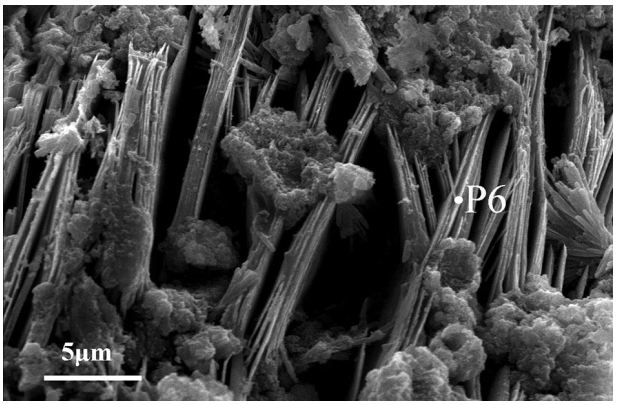

g)

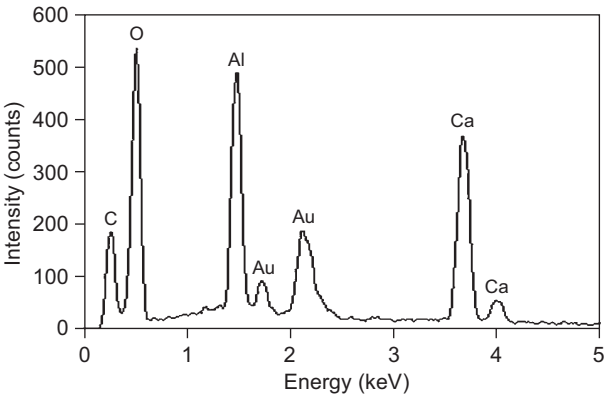

h)

Figure 5. SEM images and EDS patterns of the BCSA pastes: a), c) SEM images of the paste after curing age of 7 days; b), d) EDS patterns for P 3 and P 4 respectively; e), g) SEM images of the paste after curing age of 28 days; f), h) EDS patterns for P 5, P 6.

CONCLUSIONS

- $C_4A_3\check{S}$ and C_2S in BCSA cement possess good crystallinity and have polygonal and spherical morphologies respectively.
- Large amounts of water significantly accelerates the hydration and carbonation reaction. Especially, it promotes the formation of C_2ASH_8 and H_c in the later stages.
- C_2ASH_8 is thick hexagonal plate product and H_c is thin sheet-like product in the early stages. Massive thick plates gather together in the later stages. Meanwhile, thin sheet-like H_c stacks together forming the lamellar structure and lamellar structure H_c will also gather together.
- C_2ASH_8 and H_c are always surrounded by AFt or gel which may be a mixture of AH_3 and C–S–H.

Acknowledgments

The authors acknowledge the financial support from Priority Academic Program Development (PAPD) of Jiangsu Higher Education Institutions, Program for Changjiang Scholars and Innovative Research Team in University (PCSIRT, IRT1146).

REFERENCES

1. Álvarez-Pinazo G., Cuesta A., García-Maté M., Santacruz I., Losilla E. R., la Torre A. G. D., León-Reina L., Aranda M. A. G.: Cem. Concr. Res. *42*, 960 (2012).
2. Winnefeld F., Barlag S.: J. therm. Anal. Calorim. *101*, 949 (2010).
3. Benarchid M. Y., Rogez J., Diouri A., Boukhari A., Aride J.: Thermochim. Acta. *433*, 183 (2005).
4. Benarchid M. Y., Rogez J.: Cem. Concr. Res. *35*, 2074 (2005).
5. Zhang L., Glasser F.: Adv. Cem. Res. *14*, 141 (2002).
6. Glasser F., Zhang L.: Cem. Concr. Res. *31*, 1881 (2001).
7. Martín-Sedeño M. C., Cuberos A. J. M., De la Torre Á. G., Álvarez-Pinazo G., Ordónez L. M., Gateshki M., Aranda M. A. G.: Cem. Concr. Res. *40*, 359 (2010).
8. Adolfsson D., Viggh E., Menad N., Björkman B.: Adv. Cem. Res. *19*, 147 (2007).
9. García-Maté M., Santacruz I., De la Torre Á. G., León-Reina L., Aranda M. A. G.: Cem. Concr. Compos. *34*, 684 (2012).
10. Gartner E.: Cem. Concr. Res. *34*, 1489 (2004).
11. P. Arjunan M. R. S., Della M. Roy: Cem. Concr. Res. *29*, 1305 (1999).
12. Li H. X., Agrawal D. K., Cheng J. P., Silsbee M. R.: Cem. Concr. Res. *31*, 1257 (2001).
13. Chen I. A., Hargis C. W., Juenger M. C. G.: Cem. Concr. Res. *42*, 51 (2012).
14. Winnefeld F., Lothenbach B.: Cem. Concr. Res. *40*, 1239 (2010).
15. Chen I. A., Juenger M. C. G.: J. Mater. Sci. *46*, 2568 (2010).
16. Pelletier L., Winnefeld F., Lothenbach B.: Cem. Concr. Compos. *32*, 497 (2010).
17. Le Saoût G., Lothenbach B., Hori A., Higuchi T., Winnefeld F.: Cem. Concr. Res. *43*, 81 (2013).
18. Ma B., Li X., Mao Y., Shen X.: Ceram. Silik *57*, 7 (2013).
19. Ding J., Fu Y., Beaudoin J.: ACI Mater. J. *94*, 220 (1997).
20. Ding J., Fu Y., Beaudoin J.: Adv. Cem. Res. *7*, 171 (1995).
21. Ding J., Fu Y., Beaudoin J. J.: Cem. Concr. Res. *25*, 1311 (1995).
22. Berger S., Coumes C. C. D., Le Bescop P., Damidot D.: Cem. Concr. Res. *41*, 149 (2011).
23. Matschei T., Lothenbach B., Glasser F.: Cem. Concr. Res. *37*, 118 (2007).
24. Glasser F., Kindness A., Stronach S.: Cem. Concr. Res. *29*, 861 (1999).
25. Sánchez-Herrero M. J., Fernández-Jiménez A., Palomo A.: Cem. Concr. Res. *46*, 41 (2013).
26. Dovál M. P., Kovár V.: Ceram.-Silik. *49*, 104 (2004).
27. Zhou Q., Glasser F.: Adv. Cem. Res. *12*, 131 (2000).
28. Pelletier-Chaignat L., Winnefeld F., Lothenbach B., Müller C. J.: Constr. Build. Mater. *26*, 619 (2012).
29. Pelletier-Chaignat L., Winnefeld F., Lothenbach B., Saout G. L., Müller C. J., Famy C.: Cem. Concr. Compos. *33*, 551 (2011).
30. Puertas F., Blanco-Varela M., Vazquez T.: Cem. Concr. Res. *29*, 1673 (1999).